Article

Dicyanoisophorone-Based Near-Infrared Emission Fluorescent Probe for Detecting NAD(P)H in Living Cells and *in Vivo*

Yuehui Zhao, Keyan Wei, Fanpeng Kong, Xiaonan Gao, Kehua Xu, and Bo Tang

Anal. Chem., **Just Accepted Manuscript** • DOI: 10.1021/acs.analchem.8b03563 • Publication Date (Web): 11 Dec 2018

Dicyanoisophorone-Based Near-Infrared Emission Fluorescent Probe for Detecting NAD(P)H in Living Cells and *in Vivo*

Yuehui Zhao, Keyan Wei, Fanpeng Kong, Xiaonan Gao, Kehua Xu* and Bo Tang*

College of Chemistry, Chemical Engineering and Materials Science, Key Laboratory of Molecular and Nano Probes, Ministry of Education, Collaborative Innovation Center of Functionalized Probes for Chemical Imaging in Universities of Shandong, Shandong Normal University, Jinan 250014, P. R. China.

ABSTRACT: NADH and NADPH are ubiquitous coenzymes in all living cells and play vital roles in numerous redox reactions in cellular energy metabolism. To accurately detect the distribution and dynamic changes of NAD(P)H under physiological condition is essential for understanding its biological functions and pathological roles. In this work, we developed a near-infrared (NIR) emission fluorescent small-molecule probe (**DCI-MQ**) composed of a dicyanoisophorone chromophore conjugated with a quinolinium moiety for *in vivo* NAD(P)H detection. **DCI-MQ** owns the advantages of high water solubility, rapid response, extraordinary selectivity, great sensitivity (detection limit of 12 nM), low cytotoxicity and a NIR emission (660 nm) in response to NAD(P)H. Moreover, the probe **DCI-MQ** was successfully applied for the detection and imaging of endogenous NAD(P)H in both living cells and tumor-bearing mice, which provides an effective tool for the study of NAD(P)H-related physiological and pathological processes.

Nicotinamide adenine dinucleotide (NAD), reduced nicotinamide adenine dinucleotide (NADH), nicotinamide adenine dinucleotide phosphate (NADP), and reduced nicotinamide adenine dinucleotide phosphate (NADPH) are ubiquitous coenzymes in all living organisms. Electron carriers, NAD(P)H, are involved in many biological processes, including energy metabolism, mitochondrial function, gene expression, calcium homeostasis, antioxidation, carcinogenesis, cell death and aging.[1-7] The level changes of NAD(P)H is also associated with different pathological states, such as diabetes, cancer and neurodegeneration.[1,8-10] Therefore, dynamic monitoring and imaging of intracellular NAD(P)H are imperative for understanding the contributions of NAD(P)H in physiological and pathological processes.

Numerous classical methods for the detection of NAD(P)H *in vitro* have been reported, including electrochemical analysis,[11,12] enzymatic cycling assay,[13] high performance liquid chromatography,[14] and capillary electrophoresis.[15] For imaging of the intracellular NAD(P)H, single-photon or two-photon excitation microscopy were used based on autofluorescence of NAD(P)H.[16,17] However, the above methods are still limited by their low sensitivity, easily ultraviolet irradiation photodamage, and biomaterials' interference in cells. Fluorescence bioimaging offers a powerful tool for visualizing various biologically relevant species in living cells and animals with high resolution.[18-21] Recently, genetically encoded fluorescent sensors and nanosensors for dynamic monitoring and imaging of intracellular NAD(P)H have also been developed.[22-26] Up to date, several conveniently used small-molecule fluorescent NAD(P)H probes have been reported. Komatsu *et al.* developed a turn-off ubiquinone-rhodol fluorescent probe **UQ-Rh** ($\lambda_{ex}/\lambda_{em}$ = 492/518 nm) for imaging intracellular NAD(P)H with Ir complex as a promoter.[27] Inspired by the enzyme-catalyzed reaction, Chang's group has designed a boronic acid-containing fluorescent NADH probe based on resazurin, in which boronic acid was selected as the binding site of NADH and accelerate the reduction process of weakly fluorescent resazurin to strongly fluorescent resorufin.[28] In addition, fluorescent probes based on coumarin,[29] fluorescein,[30] cyanine,[31] calix[4]arene dimer,[32] and others,[33,34] also have been reported. However, most of them possess short emission wavelengths that hinder their application in living systems (Table S1). Up to now, organic small-molecule fluorescent probes suitable for real-time detection and imaging of NAD(P)H *in vivo* is still urgently needed. Near-infrared (NIR) range from 650–900 nm becomes most optical for *in vivo* imaging due to its less cell damage, low background autofluorescence and high tissue penetration depth.[35,36] Therefore, designing NIR fluorescent probes for imaging of NAD(P)H in living cells and *in vivo* is still quite challenging but extremely significant.

In this regard, a turn-on NIR emission fluorescent probe for the detection of NAD(P)H was developed (**DCI-MQ**, Scheme 1). The probe contains dicyanoisophorone as the NIR fluorescent chromophore and 1-methylquinolinium cation as the NAD(P)H recognition unit. Dicyanoisophorone-based fluorescent dyes have a

typical push-pull structure, NIR emission wavelength and large Stokes shift, hence many NIR fluorescent probes based on dicyanoisophorone have been reported for Au^{3+}, H_2S, biothiols, leucine aminopeptidase and HOCl.[37-41] The **DCI-MQ** displays a rapid and specific response to NAD(P)H: in the presence of NAD(P)H, the quinolinium moiety was specially reduced, and the electron-rich amine moiety was released, then a strong fluorescence was emitted at 660 nm (Stocks shift 92 nm) with a low detection limit of 12 nM. **DCI-MQ** was then successfully applied in bioimaging of endogenous NAD(P)H in living cells and *in vivo*. To the best of our knowledge, the probe **DCI-MQ** is the first NIR emission fluorescent probe for real-time imaging of endogenous NAD(P)H in tumor-bearing mice, and the probe provides a contributing tool for monitoring changes of NAD(P)H in biosystems.

Scheme 1. DCI-MQ for Fluorescent Detection of NAD(P)H

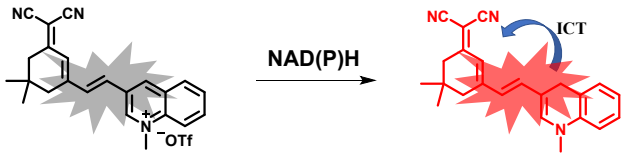

EXPERIMENTAL SECTION

Synthesis of DCI-MQ. *Synthesis of Compound* ***1***. To a solution of isophorone (2.1 mL, 13.8 mmol) and malononitrile (0.91 g, 13.8 mmol) in 30 mL anhydrous ethanol, catalytic amount of piperidine (14 μL, 0.14 mmol) was added. The mixture was stirred at 60 °C for 8 h. After cooling to room temperature, the mixture was slowly transfered into 50 mL water and the precipitated solid was filtered to give product **1** (1.2 g, yield 47%). ^{1}H NMR (Chloroform-*d*, 400 MHz): δ = 6.60 (s, 1H), 2.50 (s, 2H), 2.16 (s, 2H), 2.02 (s, 3H), 1.00 (s, 6H); ^{13}C NMR (Chloroform-*d*, 101 MHz): δ = 170.44, 159.87, 120.56, 113.19, 112.41, 78.17, 45.66, 42.63, 32.37, 27.81, 25.32. HRMS: (ESI, *m*/*z*) calcd for $C_{12}H_{14}N_2$, $[M - H]^-$: 185.1073, found: 185.1082.

Synthesis of Compound ***2***. Compound **1** (200 mg, 1.07 mmol), 3-quinolinecarboxaldehyde (202 mg, 1.28 mmol) and catalytic amount of piperidine (11 μL, 0.11 mmol) were dissolved in 8 mL dry acetonitrile. The mixture was stirred at 50 °C for 5 h. After cooling to room temperature, the precipitate was filtered to obtain the desired product **2** (150 mg, yield 43%). ^{1}H NMR (DMSO-d_6, 400 MHz): δ = 9.24 (s, 1H), 8.64 (s, 1H), 8.03 (d, *J* = 8.4 Hz, 1H), 7.97 (d, *J* = 8.2 Hz, 1H), 7.78 (t, *J* = 7.7 Hz, 1H), 7.72 (d, *J* = 16.3 Hz, 1H), 7.65 (t, *J* = 7.6 Hz, 1H), 7.49 (d, *J* = 16.3 Hz, 1H), 6.96 (s, 1H), 2.64 (s, 2H), 2.60 (s, 2H), 1.04 (s, 6H); ^{13}C NMR (DMSO-d_6, 101 MHz): δ = 170.72, 155.67, 150.49, 147.95, 134.61, 134.57, 131.89, 130.75, 129.70, 129.29, 129.00, 127.98, 127.81, 124.08, 113.40, 77.69, 42.72, 38.52, 32.18, 27.93. HRMS: (ESI, *m*/*z*) calcd for $C_{22}H_{19}N_3$, $[M + H]^+$: 326.1651, found: 326.1657.

Synthesis of the probe ***DCI-MQ***. Compound **2** (60 mg, 0.18 mmol) and methyl trifluoromethanesulphonate (0.1 mL, 0.92 mmol) were added into 5 mL chloroform. The mixture was stirred at room temperature under a nitrogen atmosphere for 24 hours. Afterwards, the solvent was removed under reduced pressure, and 10 mL ether was added to precipitate the desired product **DCI-MQ** as a yellow solid. Yield: 70 mg (70%). ^{1}H NMR (DMSO-d_6, 400 MHz): δ = 9.89 (s, 1H), 9.40 (s, 1H), 8.51 (d, *J* = 8.9 Hz, 1H), 8.39 (d, *J* = 8.3 Hz, 1H), 8.27 (t, *J* = 8.7 Hz, 1H), 8.07 (t, *J* = 7.6 Hz, 1H), 7.77 (d, *J* = 16.3 Hz, 1H), 7.52 (d, *J* = 16.3 Hz, 1H), 6.96 (s, 1H), 4.64 (s, 3H), 2.70 (s, 2H), 2.60 (s, 2H), 1.07 (s, 6H); ^{13}C NMR (DMSO-d_6, 101 MHz): δ = 170.36, 154.13, 150.08, 143.73, 137.90, 135.97, 134.84, 131.04, 130.97, 130.67, 129.45, 125.59, 119.77, 113.82, 113.17, 79.46, 46.20, 42.60, 38.47, 32.24, 27.88. HRMS: (ESI, *m*/*z*) calcd for $C_{24}H_{22}F_3N_3O_3S$, $[M - TfO]^+$: 340.1808, found: 340.1802.

Scheme 2. Synthesis of DCI-MQ

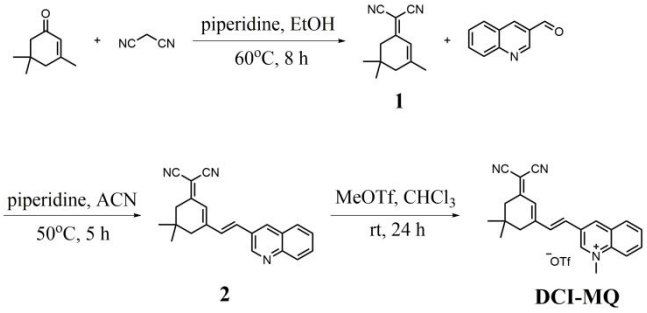

***In Vitro* Detection of NADH.** The stock solution of **DCI-MQ** (2×10^{-3} M) was prepared in DMSO. Stock solutions of NAD(P)H and various interferential reagents (K^+, Na^+, Ca^{2+}, Mg^{2+}, Zn^{2+}, Fe^{3+}, Fe^{2+}, glycine, lysine, methionine, serine, cysteine, homocysteine, glutathione, Vitamin C, dithiothreitol, H_2O_2, NaClO, *t*-BuOOH and NO) were prepared in double-distilled water, while superoxide ($O_2^{\bullet-}$) was prepared from a solution of KO_2 in DMSO. For spectral measurements, the stock solution of the probe was diluted with PBS buffer (10 mM, pH = 7.4) to give a final concentration of 10 μM. NAD(P)H and various analytes were added to the solution of **DCI-MQ** (10 μM) in PBS buffer (10 mM, pH = 7.4, containing 0.5% DMSO). The UV-Vis absorption spectra were collected from 280–700 nm, and the fluorescence emission spectra were recorded in a range from 592–800 nm (λ_{ex} = 568 nm, λ_{em} = 660 nm, slit widths: 10 nm/10 nm).

Cell Culture and Fluorescence Imaging. HepG2 and HL-7702 cells were cultured in DMEM (Dulbecco's modified Eagle's medium) supplemented with 1% penicillin-streptomycin, 10% fetal bovine serum at 37 °C in an incubator of 5% CO_2. The cells were incubated in confocal dishes for 12 h to adhere, and then the solution of **DCI-MQ** in DMSO was added to the adherent cells to give a final concentration of 10 μM **DCI-MQ**. All fluorescence images were acquired by a Leica TCS SP8 confocal laser scanning microscopy with a 63× oil objective lens. Time-dependent images were acquired every five minutes after addition of 10 μM **DCI-MQ** into HepG2 cells. To compare the difference of NADH content between tumor cells and normal cells, HepG2 cells and HL-7702 cells were respectively treated with 10 μM **DCI-**

MQ for 15 min, washed three times with PBS buffer. For glucose stimulation, HepG2 cells were pretreated with 20 mM glucose for 30 min, and then treated with 10 μM **DCI-MQ** for 15 min. For colocalization assay, HepG2 cells or HL-7702 cells were co-stained with 10 μM **DCI-MQ** and 1 μM Mito-Tracker Green for 15 min. **DCI-MQ** (red channel) was excited at 561 nm and the fluorescence emission range was set from 590 to 700 nm. Mito-Tracker Green (green channel) was excited at 488 nm and the fluorescence emission range was set from 500 to 550 nm.

RESULTS AND DISCUSSION

Design and Synthesis of DCI-MQ. The reduction of 1-methylquinolinium cations followed previously report, which bearing an electron-withdrawing substituent in the 3-positon, with NADH analogues to yield the 1,4-dihydroquinolines predominantly.[42] In this regard, the probe **DCI-MQ** was designed using quinolinium moiety as the reduction site of NAD(P)H and the dicyanoisophorone electron-withdrawing group as the NIR chromophore. It is envisioned that, upon reaction with NAD(P)H, quinolinium moiety could be reduced into an electron-rich amine moiety, and the reaction product possesses an intramolecular charge transfer (ICT) process, thereby leading to a distinct NIR fluorescence signal. Consequently, the probe was conveniently prepared in three steps and purified by filtration (Scheme 2), and all the products were characterized by nuclear magnetic resonance (^{1}H NMR, ^{13}C NMR) and high-resolution mass spectrometry (HRMS), as shown in the Experimental Section and Supporting Information.

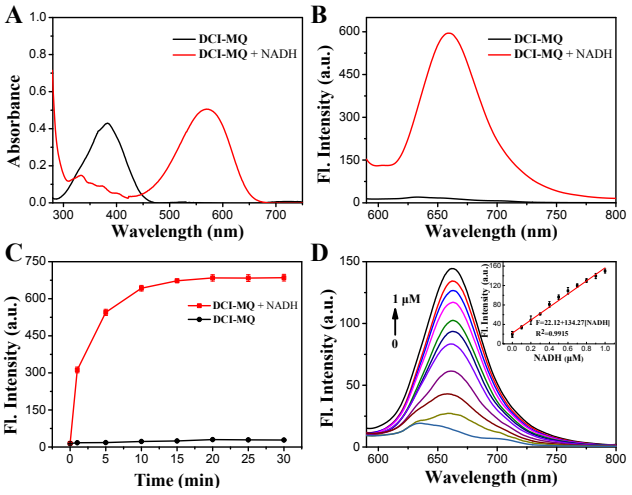

Figure 1. (A) UV-Vis absorption and (B) fluorescence emission spectra of **DCI-MQ** (10 μM) before and after reaction with NADH (50 μM). (C) The time-dependent fluorescence intensities at 660 nm of **DCI-MQ** (10 μM) with NADH (50 μM) in PBS buffer (10 mM, pH 7.4, 0.5% DMSO). (D) Fluorescence response of **DCI-MQ** (10 μM) after incubated with different concentration of NADH (0–1 μM) in PBS buffer (10 mM, pH 7.4, 0.5% DMSO) at 37 °C for 15 min. Inset: Linear fitting curve of the fluorescence intensity at 660 nm towards the concentration of NADH (0–1 μM). $\lambda_{ex}/\lambda_{em}$ = 568/660 nm. Error bars represent standard deviation (n = 3).

Optical Properties. To testify the detection sensitivity of the probe towards NADH, the optical properties in the presence/absence of NADH were measured in PBS buffer (10 mM, pH = 7.4, containing 0.5% DMSO, v/v). From the UV-Vis spectra, **DCI-MQ** exhibits a maximum absorption wavelength at 380 nm in the presence of NADH, and then redly shifted to 568 nm after reaction with NADH (Figure 1A). Concurrently, the fluorescence emission spectral of **DCI-MQ** treated with NADH have also enhanced significantly at 660 nm (Quantum Yield = 0.16) (Figure 1B). Both changes can be attributed to the reduction of quinolinium moiety, which transfers the probe to a typical donor-π-acceptor (D-π-A) structure and for producing remarkable fluorescence signal. The time-dependent (0–30 min) fluorescence response of **DCI-MQ** with NADH (50 μM) was tested (Figure 1C): the fluorescence intensity at 660 nm of **DCI-MQ** (10 μM) exhibits negligible changes, whereas it rapidly intensified to a plateau at 15 min after the treatment of NADH. These results prove that **DCI-MQ** is an ideal turn-on NIR emission fluorescent probe for detecting NADH.

Quantification of NADH and Detection Limit. Fluorescent titration experiments of **DCI-MQ** to different concentration of NADH (0–1 μM) were examined to investigate the sensitivity of **DCI-MQ** toward NADH. The fluorescence emission intensities at 660 nm enhanced gradually, and exhibit excellent linearity when plotting versus the concentration of NADH (Figure 1D). The regression equation is F = 22.12 + 134.27 [NADH], with a linear coefficient of 0.9915, and the limit of detection (signal to noise ratio = 3) for NADH was further calculated as low as 12 nM. The probe's fluorescence intensities after addition of different concentrations of NADH (0–50 μM) was also observed (Figure S1), which agrees with the performance of the previous study also. Hence, **DCI-MQ** with excellent sensitivity to NADH applies as an effective tool for imaging endogenous NADH in biological samples.

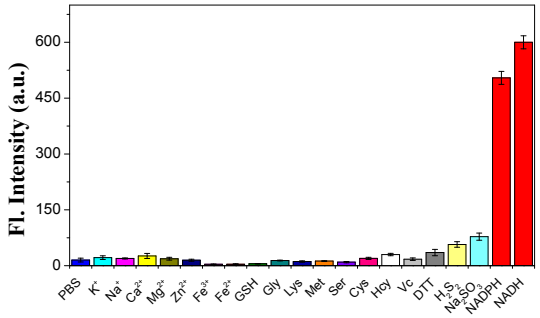

Figure 2. Fluorescence intensity of 10 μM **DCI-MQ** at 660 nm in the presence of various analytes: 1 mM of (K^+, Na^+, Ca^{2+}, Mg^{2+}, Zn^{2+}, Fe^{3+}, Fe^{2+}, GSH, Gly, Lys, Met, Ser); 100 μM of (Cys, Hcy, VC, DTT); 5 μM of (H_2S_2, Na_2SO_3); and 50 μM of (NADPH, NADH). Error bars represent standard deviation (n = 3).

Selectivity of DCI-MQ. Before applying the probe to complicated biological sample, the selectivity of **DCI-MQ** toward NAD(P)H was investigated by fluorescence

measurements of the probe to other biological relevant species in PBS buffer, including inorganic salts (K^+, Na^+, Ca^{2+}, Mg^{2+}, Zn^{2+}, Fe^{3+}, Fe^{2+}), common amino acids (glycine, lysine, methionine, serine, cysteine, homocysteine), and reducing agents (glutathione, Vitamin C, dithiothreitol, H_2S_2 and SO_3^{2-}). The fluorescence intensities at 660 nm only increased dramatically when NAD(P)H was added, but all the other analytes occupied quite low response (Figure 2). Notably, sulfite has considerably higher fluorescence intensity change than other materials,[43] but still negligible to NAD(P)H due to its low *in vivo* concentration (0.2 and 4.87 μM).[44-48] Meanwhile, after **DCI-MQ** reacted with NADH, the fluorescence intensities yielded a negligible change after various reactive oxygen species (ROSs) addition, including $O_2^{\bullet-}$, H_2O_2, NaClO, *t*-BuOOH and NO (Figure S2), which represents the reaction product also owns high stability. These data further validates that **DCI-MQ** possesses a high selectivity for NAD(P)H under physiological conditions and therefore could be potentially used to specific NAD(P)H detection in biological samples.

Scheme 3. Proposed Reaction Mechanism for the Response of DCI-MQ to NADH

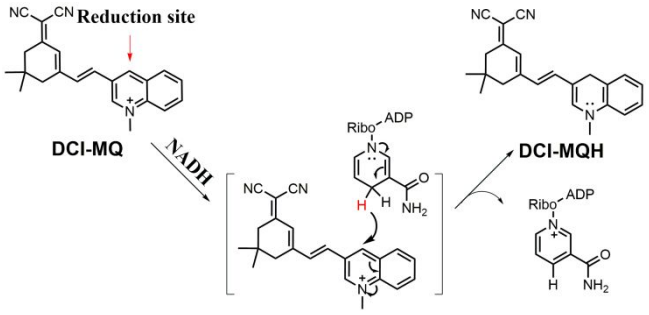

Reaction Mechanism and pH Influence. The proposed mechanism for the response of **DCI-MQ** to NADH is that the quinolinium moiety can be reduced to the 1, 4-dihydroquinoline by reacting with NADH (Scheme 3). In order to explore the reductive sensing mechanism, the probe and the product of **DCI-MQ** with NADH were analyzed by ESI-HRMS and ^{1}H NMR spectroscopy. After completing reaction of the probe with NADH in PBS buffer, the product was extracted with dichloromethane and then purified by silica gel column chromatography. The reaction product, **DCI-MQH**, was observed by the $[M - H]^-$ signal at m/z = 340.1855 (Figure S3, calculated for $[M - H]^-$ $C_{23}H_{23}N_3$: 340.1808). To further confirm the proposed mechanism, ^{1}H NMR spectroscopy of **DCI-MQ** and **DCI-MQH** was also carried out. The reduction of quinolinium induced pronounced upfield shift of N-CH_3 from 4.64 to 3.27 ppm, and a new singlet at 3.72 ppm emerged clearly (Figure S4). In addition, the HPLC analysis was also performed in order to explain the mechanism. After the reaction of **DCI-MQ** with NADH, a new peak at 7.87 min belonging to reaction product (**DCI-MQH**) was observed, and the peak at 5.17 min corresponding to **DCI-MQ** decreased remarkably (Figure S5). Hereafter, these data confirmed the reductive sensing mechanism of **DCI-MQ** with NADH. Besides, the pH influence on the fluorescence response of **DCI-MQ** with NADH was also investigated in PBS buffer (pH = 5.8–8.0), which indicated that the probe is capable of detecting NAD(P)H under physiological pH conditions (Figure S6).

Cytotoxicity Assays. Prior to analysis in living cells, we tested the cytotoxicity of **DCI-MQ** using a conventional MTT assay in HepG2 cells. In Figure S7, HepG2 cells kept higher viability when incubated with 0–100 μM of **DCI-MQ** for 12 h, thereby validating that **DCI-MQ** holds low cytotoxicity to cells at the concentration of 10 μM for 12 h under experimental conditions, and it is potentially applicable for the biological application.

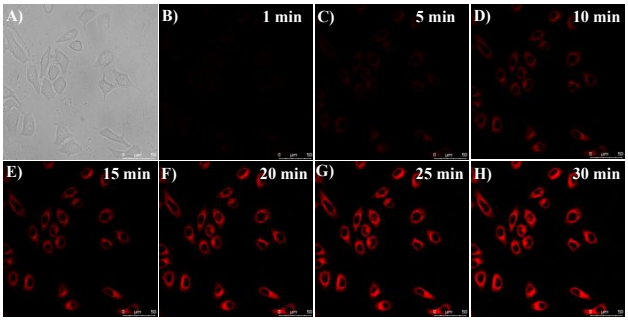

Figure 3. Time-dependent fluorescence imaging of endogenous NADH in HepG2 cells incubated with **DCI-MQ** (10 μM) for 30 min. (A) Bright filed and (B-H) fluorescence images of HepG2 cells captured without washing. Cell images were acquired with $\lambda_{ex}/\lambda_{em}$ of 561/590–700 nm. Scale bar: 50 μm.

Fluorescence imaging in living cells. Encouraged by the above satisfactory outcome, we further investigated the imaging ability of **DCI-MQ** for endogenous NAD(P)H. HepG2 cells were treated with **DCI-MQ** (10 μM) and recorded their fluorescence changes within 30 min using confocal analysis. After addition of **DCI-MQ**, the NIR fluorescence signal of HepG2 cells increased gradually in 30 min, and almost no fluorescence outside the cells was observed even without washing (Figure 3). In addition, a control experiment with H_2O_2 was carried out. The HepG2 cells were pretreated with 100 μM H_2O_2 for 30 min and then treated with 10 μM probe for 30 min. The fluorescence intensity of HepG2 cells decreased obviously duo to the lower NADH level in the process of H_2O_2-induced oxidative stress (Figure S8).[15] The result indicated that the probe has decent cell permeability and could react with endogenous NAD(P)H in living cells.

Recent studies have shown that the ratio of NAD^+/NADH is significantly lower in certain tumor cell lines, representing that the level of NADH in tumor cells is higher than normal cells.[20] To compare the difference of NADH content between tumor cells and normal cells, we investigated the fluorescence signal intensity in tumor cells (HepG2 cells) and normal cells (HL-7702 cells) by **DCI-MQ**. The fluorescence intensity in HepG2 cells was much stronger than in HL-7702 cells (Figure 4), verifying the concentration level of NADH in HepG2 cells was higher than in HL-7702 cells. The data suggests that the probe is capable of tracking endogenous NADH in living

cells and reveals the different NADH content between tumor cells and normal cells.

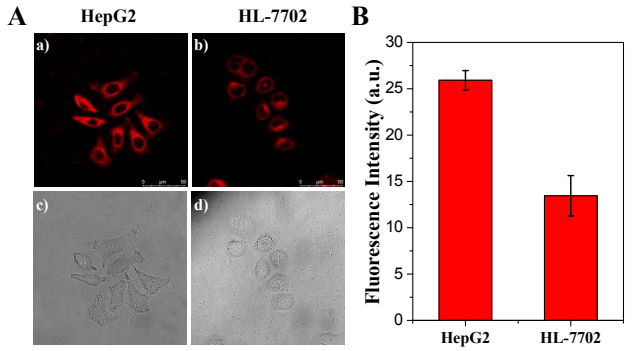

Figure 4. (A) Fluorescence and bright field images of HepG2 cells (a, c) and HL-7702 cells (b, d) incubated with **DCI-MQ** (10 μM) for 15 min, respectively. (B) Quantified fluorescence intensities of (a) and (b). Cell images were acquired with $\lambda_{ex}/\lambda_{em}$ of 561/590–700 nm. Scale bar: 50 μm.

In tumor cells, the intracellular NADH level is mainly dependent on the glycolysis, which consumes glucose and generates NADH. Therefor the addition of glucose can elevate the intracellular NADH level. HepG2 cells were firstly pretreated with 20 mM glucose for 30 min, and then incubated with 10 μM **DCI-MQ** for another 15 min before confocal imaging. As expected, the fluorescence signal intensity of **DCI-MQ** stained cells was enhanced after incubation with 20 mM glucose (Figure 5).

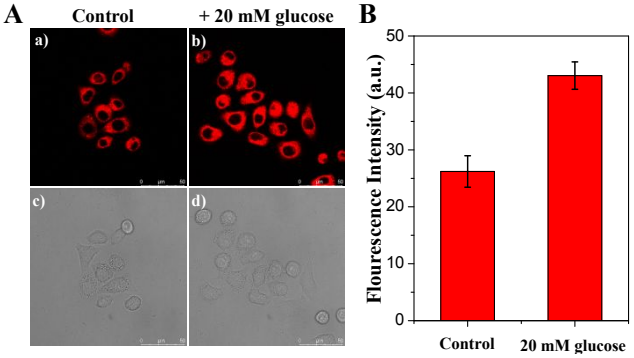

Figure 5. (A) Fluorescence and bright field images of endogenous NAD(P)H in HepG2 cells: (a, c) Cells stained with **DCI-MQ** (10 μM, 15 min), (b, d) Cells pretreated with glucose (20 mM, 30 min) and then stained with **DCI-MQ** (10 μM, 15 min), respectively. (B) Quantified fluorescence intensities of (a) and (b). Cell images were acquired with $\lambda_{ex}/\lambda_{em}$ of 561/590–700 nm. Scale bar: 50 μm.

A photobleaching test was performed for study the photostability of the reaction product in living cells by using confocal laser scanning microscopy. Within 600 s, the fluorescence signal remains unchanged (Figure S9), signifying that the reaction product with great photostability. The subcellular distribution of **DCI-MQ** was also completed by co-staining HepG2 cells or HL-7702 cells with **DCI-MQ** and Mito-Tracker Green, a typical commercially available mitochondrial tracker. Figure 6 displays the overlapped fluorescence intensities (Pearson's colocalization coefficient 0.85 for HepG2 cells and 0.91 for HL-7702 cells) of Mito-Tracker Green and **DCI-MQ** merged well, which designated that quinolinium moiety did bring **DCI-MQ** to the mitochondria of living cells. The colocalization experiments indicated that the probe was organelle-specifically trapped in the mitochondria of living cells.

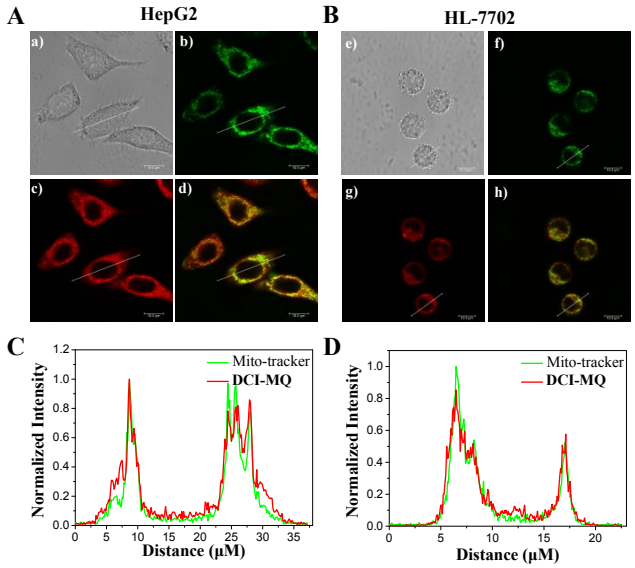

Figure 6. Intracellular localization of HepG2 and HL-7702 cells incubated with **DCI-MQ**. (A) & (B) CLSM images of cells pretreated with 10 μM **DCI-MQ** and 1 μM Mito-Tracker Green for 15 min. (a) (e) Bright filed; (b) (f) green channel, Mito-Tracker Green; (c) (g) red channel, probe fluorescence; (d) (h) the overlap (b) (f) and (c) (g) respectively. (C) & (D) Intensity profile of ROIs across HepG2 and HL-7702 cells respectively. Scale bar: 10 μm.

Imaging of NAD(P)H *in Vivo*. The current small-molecule fluorescent NAD(P)H probes with emission wavelengths located in the visible region are not suitable for *in vivo* images. Therefore, to evaluate the suitability of **DCI-MQ** to respond to NAD(P)H *in vivo*, Kunming mice with homograft murine hepatoma cell line H22 tumor were orthotopically injected with buffer solutions containing **DCI-MQ** (10 μM) and then fluorescence images were obtained at different times using a small animal *in vivo* imaging system (IVIS). The fluorescence signal was gradually intensified in the tumor region, indicating that the probe can detect endogenous NAD(P)H in H22 tumor-bearing mice (Figure 7). In this regard, it can be concluded that **DCI-MQ** is an effective probe for imaging endogenous NAD(P)H at the organism level.

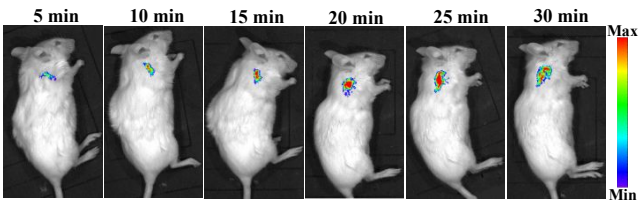

Figure 7. *In vivo* fluorescence images of H22 tumor-bearing mice injected with **DCI-MQ** (10 μM, 100 μL) *via*

orthotopically injection for 30 min. $\lambda_{ex}/\lambda_{em}$ of 560/670 nm was applied.

CONCLUSIONS

In conclusion, a novel dicyanoisophorone-based fluorescent NAD(P)H probe, **DCI-MQ**, with near-infrared emission has been developed successfully on the basis of a specific reduction. **DCI-MQ** exhibits high NAD(P)H selectivity over other biologically relevant species, as well as a significantly low detection limit of 12 nM. With the low cytotoxicity and great cell membrane permeability, **DCI-MQ** was successfully applied for bioimaging of endogenous NAD(P)H in living cells and *in vivo*. As for its easy preparation, **DCI-MQ** shows substantial potential for applications in the study of the physiological and pathological roles of NAD(P)H, and provides an effective tool for monitoring changes of NAD(P)H level in reductive stress in our future works.

ASSOCIATED CONTENT

Supporting Information

Materials and instruments, experimental details, supplementary data and characterization figures of compounds. The Supporting Information is available free of charge *via* the Internet at http://pubs.acs.org.

AUTHOR INFORMATION

Corresponding Author

*Phone: 86-531-86180010
*E-mail: xukehua@sdnu.edu.cn; tangb@sdnu.edu.cn

Author Contributions

All authors have given approval to the final version of the manuscript.

Notes

The authors declare no competing financial interests.

ACKNOWLEDGMENT

This work was supported by National Natural Science Foundation of China (21575081, 21535004, 21775091, 91753111 and 21705098) and the Key Research and Development Program of Shandong Province (2018YFJH0502).

REFERENCES

(1) Eto, K.; Tsubamoto, Y.; Terauchi, Y.; Sugiyama, T.; Kishimoto, T.; Takahashi, N.; Yamauchi, N.; Kubota, N.; Murayama, S.; Aizawa, T.; Akanuma, Y.; Aizawa, S.; Kasai, H.; Yazaki, Y.; Kadowaki, T. Role of NADH shuttle system in glucose-induced activation of mitochondrial metabolism and insulin secretion. *Science* **1999**, *283*, 981-985.

(2) Kaplin, A.; Snyder, S.; Linden, D. Reduced nicotinamide adenine dinucleotide-selective stimulation of inositol 1,4,5-trisphosphate receptors mediates Hypoxic mobilization of calcium. *J. Neurosci.* **1996**, *16*, 2002-2011.

(3) Kirsch, M.; Groot, H. D. NAD(P)H, a directly operating antioxidant? *FASEB J.* **2001**, *15*, 1569-1574.

(4) Lin, S.-J.; Ford, E.; Haigis, M.; Liszt, G.; Guarente, L. Calorie restriction extends yeast life span by lowering the level of NADH. *Genes Dev.* **2004**, *18*, 12-16.

(5) Rutter, J.; Reick, M.; Wu, L. C.; McKnight, S. L. Regulation of clock and NPAS2 DNA binding by the redox state of NAD cofactors. *Science* **2001**, *293*, 510-514.

(6) Seimiya, H.; Muramatsu, Y.; Ohishi, T.; Tsuruo, T. Tankyrase 1 as a target for telomere-directed molecular cancer therapeutics. *Cancer Cell* **2005**, *7*, 25-37.

(7) Zhang, Q.; Piston, D. W.; Goodman, R. H. Regulation of corepressor function by nuclear NADH. *Science* **2002**, *295*, 1895-1897.

(8) Nóbrega-Pereira, S.; Fernandez-Marcos, P. J.; Brioche, T.; Gomez-Cabrera, M. C.; Salvador-Pascual, A.; Flores, J. M.; Viña, J.; Serrano, M. G6PD protects from oxidative damage and improves healthspan in mice. *Nat. Commun.* **2016**, *7*, 10894.

(9) Zhang, Q.; Wang, S.-Y.; Nottke, A. C.; Rocheleau, J. V.; Piston, D. W.; Goodman, R. H. Redox sensor CtBP mediates hypoxia-induced tumor cell migration. *Proc. Natl. Acad. Sci. USA* **2006**, *103*, 9029-9033.

(10) Schulze, A.; Harris, A. L. How cancer metabolism is tuned for proliferation and vulnerable to disruption. *Nature* **2012**, *491*, 364-373.

(11) Govindhan, M.; Amiri, M.; Chen, A. Au nanoparticle/graphene nanocomposite as a platform for the sensitive detection of NADH in human urine. *Biosens. Bioelectron.* **2015**, *66*, 474-480.

(12) Istrate, O.-M.; Rotariu, L.; Marinescu, V. E.; Bala, C. NADH sensing platform based on electrochemically generated reduced graphene oxide–gold nanoparticles composite stabilized with poly (allylamine hydrochloride). *Sens. Actuators, B* **2016**, *223*, 697-704.

(13) Cook, D. B.; Self, C. H. Determination of one thousandth of an attomole (1 zeptomole) of alkaline phosphatase: application in an immunoassay of proinsulin. *Clin. Chem.* **1993**, *39*, 965-971.

(14) Yang, H.; Yang, T.; Baur, J. A.; Perez, E.; Matsui, T.; Carmona, J. J.; Lamming, Dudley W.; Souza-Pinto, N. C.; Bohr, V. A.; Rosenzweig, A.; de Cabo, R.; Sauve, Anthony A.; Sinclair, D. A. Nutrient-sensitive mitochondrial NAD^+ levels dictate cell survival. *Cell* **2007**, *130*, 1095-1107.

(15) Xie, W.; Xu, A.; Yeung, E. S. Determination of NAD+ and NADH in a single cell under hydrogen peroxide stress by capillary electrophoresis. *Anal. Chem.* **2009**, *81*, 1280-1284.

(16) Patterson, G. H.; Knobel, S. M.; Arkhammar, P.; Thastrup, O.; Piston, D. W. Separation of the glucose-stimulated cytoplasmic and mitochondrial NAD(P)H responses in pancreatic islet β cells. *Proc. Natl. Acad. Sci. USA* **2000**, *97*, 5203-5207.

(17) Skala, M. C.; Riching, K. M.; Gendron-Fitzpatrick, A.; Eickhoff, J.; Eliceiri, K. W.; White, J. G.; Ramanujam, N. In vivo multiphoton microscopy of NADH and FAD redox states, fluorescence lifetimes, and cellular morphology in precancerous epithelia. *Proc. Natl. Acad. Sci. USA* **2007**, *104*, 19494-19499.

(18) O'Connor, J. P. B.; Aboagye, E. O.; Adams, J. E.; Aerts, H. J. W. L.; Barrington, S. F.; Beer, A. J.; Boellaard, R.; Bohndiek, S. E.; Brady, M.; Brown, G.; Buckley, D. L.; Chenevert, T. L.; Clarke, L. P.; Collette, S.; Cook, G. J.; deSouza, N. M.; Dickson, J. C.; Dive, C.; Evelhoch, J. L.; Faivre-Finn, C.; Gallagher, F. A.; Gilbert, F. J.; Gillies, R. J.; Goh, V.; Griffiths, J. R.; Groves, A. M.; Halligan, S.; Harris, A. L.; Hawkes, D. J.; Hoekstra, O. S.; Huang, E. P.; Hutton, B. F.; Jackson, E. F.; Jayson, G. C.; Jones, A.; Koh, D.-M.; Lacombe, D.; Lambin, P.; Lassau, N.; Leach, M. O.; Lee, T.-Y.; Leen, E. L.; Lewis, J. S.; Liu, Y.; Lythgoe, M. F.; Manoharan, P.; Maxwell, R. J.; Miles, K. A.; Morgan, B.; Morris, S.; Ng, T.; Padhani, A. R.; Parker, G. J. M.; Partridge, M.; Pathak, A. P.; Peet, A. C.; Punwani, S.; Reynolds, A. R.; Robinson, S. P.; Shankar, L. K.; Sharma, R. A.; Soloviev, D.; Stroobants, S.; Sullivan, D. C.; Taylor, S. A.; Tofts, P. S.; Tozer, G. M.; van Herk, M.; Walker-Samuel, S.; Wason, J.; Williams, K. J.; Workman, P.; Yankeelov,

T. E.; Brindle, K. M.; McShane, L. M.; Jackson, A.; Waterton, J. C. Imaging biomarker roadmap for cancer studies. *Nat. Rev. Clin. Oncol.* **2017**, *14*, 169-186.

(19) Katayama, Y. Peptide-grafted polymers as artificial converter of cellular signals. *Bull. Chem. Soc. Jpn.* **2017**, *90*, 12-21.

(20) Hou, J.-T.; Ren, W. X.; Li, K.; Seo, J.; Sharma, A.; Yu, X.-Q.; Kim, J. S. Fluorescent bioimaging of pH: from design to applications. *Chem. Soc. Rev.* **2017**, *46*, 2076-2090.

(21) Bhattacharyya, K.; Mukherjee, S. Fluorescent Metal Nano-Clusters as Next Generation Fluorescent Probes for Cell Imaging and Drug Delivery. *Bull. Chem. Soc. Jpn.* **2018**, *91*, 447-454.

(22) Zhao, Y.; Jin, J.; Hu, Q.; Zhou, H.-M.; Yi, J.; Yu, Z.; Xu, L.; Wang, X.; Yang, Y.; Loscalzo, J. Genetically encoded fluorescent sensors for intracellular NADH detection. *Cell Metab.* **2011**, *14*, 555-566.

(23) Bilan, D. S.; Matlashov, M. E.; Gorokhovatsky, A. Y.; Schultz, C.; Enikolopov, G.; Belousov, V. V. Genetically encoded fluorescent indicator for imaging NAD^+/NADH ratio changes in different cellular compartments. *Biochim. Biophys. Acta* **2014**, *1840*, 951-957.

(24) Zhao, Y.; Hu, Q.; Cheng, F.; Su, N.; Wang, A.; Zou, Y.; Hu, H.; Chen, X.; Zhou, H.-M.; Huang, X.; Yang, K.; Zhu, Q.; Wang, X.; Yi, J.; Zhu, L.; Qian, X.; Chen, L.; Tang, Y.; Loscalzo, J.; Yang, Y. SoNar, a highly responsive NAD^+/NADH sensor, allows high-throughput metabolic screening of anti-tumor agents. *Cell Metab.* **2015**, *21*, 777-789.

(25) Tao, R.; Zhao, Y.; Chu, H.; Wang, A.; Zhu, J.; Chen, X.; Zou, Y.; Shi, M.; Liu, R.; Su, N.; Du, J.; Zhou, H.-M.; Zhu, L.; Qian, X.; Liu, H.; Loscalzo, J.; Yang, Y. Genetically encoded fluorescent sensors reveal dynamic regulation of NADPH metabolism. *Nat. Methods* **2017**, *14*, 720-728.

(26) Freeman, R.; Gill, R.; Shweky, I.; Kotler, M.; Banin, U.; Willner, I. Biosensing and probing of intracellular metabolic pathways by NADH-sensitive quantum dots. *Angew. Chem., Int. Ed.* **2009**, *121*, 315-319.

(27) Komatsu, H.; Shindo, Y.; Oka, K.; Hill, J. P.; Ariga, K. Ubiquinone-Rhodol (UQ-Rh) for Fluorescence imaging of NAD(P)H through intracellular activation. *Angew. Chem., Int. Ed.* **2014**, *53*, 3993-3995.

(28) Wang, L.; Zhang, J.; Kim, B.; Peng, J.; Berry, S. N.; Ni, Y.; Su, D.; Lee, J.; Yuan, L.; Chang, Y.-T. Boronic Acid: A bio-inspired strategy to increase the sensitivity and selectivity of fluorescent NADH Probe. *J. Am. Chem. Soc.* **2016**, *138*, 10394-10397.

(29) A. Roeschlaub, C.; L. Maidwell, N.; Reza Rezai, M.; G. Sammes, P. A fluorescent probe for the detection of NAD(P)H. *Chem. Commun.* **1999**, 1637-1638.

(30) Jung, S. O.; Ahn, J. Y.; Kim, S.; Yi, S.; Kim, M. H.; Jang, H. H.; Seo, S. H.; Eom, M. S.; Kim, S. K.; Ryu, D. H.; Chang, S.-K.; Han, M. S. Fluorescein derivative-based, selective and sensitive chemosensor for NADH. *Tetrahedron Lett.* **2010**, *51*, 3775-3778.

(31) Fomin, M. A.; Dmitriev, R. I.; Jenkins, J.; Papkovsky, D. B.; Heindl, D.; König, B. Two-acceptor cyanine-based fluorescent indicator for NAD(P)H in tumor cell models. *ACS Sens.* **2016**, *1*, 702-709.

(32) Zadmard, R.; Akbari-Moghaddam, P.; Darvishi, S.; Mirza-Aghayan, M. A highly selective fluorescent chemosensor for NADH based on calix[4] arene dimer. *Tetrahedron* **2017**, *73*, 604-607.

(33) Tu, C.; Nagao, R.; Louie Angelique , Y. Multimodal magnetic-resonance/optical-imaging contrast agent sensitive to NADH. *Angew. Chem., Int. Ed.* **2009**, *48*, 6547-6551.

(34) Ito, H.; Terai, T.; Hanaoka, K.; Ueno, T.; Komatsu, T.; Nagano, T.; Urano, Y. Detection of NAD(P)H-dependent enzyme activity with dynamic luminescence quenching of terbium complexes. *Chem. Commun.* **2015**, *51*, 8319-8322.

(35) Guo, Z.; Park, S.; Yoon, J.; Shin, I. Recent progress in the development of near-infrared fluorescent probes for bioimaging applications. *Chem. Soc. Rev.* **2014**, *43*, 16-29.

(36) Owens, E. A.; Henary, M.; El Fakhri, G.; Choi, H. S. Tissue-specific near-infrared fluorescence imaging. *Acc. Chem. Res.* **2016**, *49*, 1731-1740.

(37) Z. Li, Y. Xu, J. Fu, H. Zhu and Y. Qian, Monitoring of Au (III) species in plants using a selective fluorescent probe. *Chem. Commun.* **2018**, *54*, 888-891.

(38) Xiang, K.; Liu, Y.; Li, C.; Tian, B.; Tong, T.; Zhang, J. A colorimetric and ratiometric fluorescent probe with a large stokes shift for detection of hydrogen sulfide. *Dyes Pigm.* **2015**, *123*, 78-84.

(39) Zhang, M.-Z.; Han, H.-H.; Zhang, S.-Z.; Wang, C.-Y.; Lu, Y.-X.; Zhu, W.-H. A new colorimetric and fluorescent probe with a large stokes shift for rapid and specific detection of biothiols and its application in living cells. *J. Mater. Chem. B* **2017**, *5*, 8780-8785.

(40) Zhang, W.; Liu, F.; Zhang, C.; Luo, J.-G.; Luo, J.; Yu, W.; Kong, L. Near-Infrared Fluorescent Probe with Remarkable Large Stokes Shift and Favorable Water Solubility for Real-Time Tracking Leucine Aminopeptidase in Living Cells and In Vivo. *Anal. Chem.* **2017**, *89*, 12319-12326.

(41) Zheng, D.; Qiu, X.; Liu, C.; Jiao, X.; He, S.; Zhao, L.; Zeng, X. Synthesis and bioapplication of a highly selective and sensitive fluorescent probe for HOCl based on a phenothiazine–dicyanoisophorone conjugate with large Stokes shift. *New J. Chem.* **2018**, *42*, 5135-5141.

(42) Bunting, J. W.; Fitzgerald, N. P. Kinetics of the reduction of 1-methylquinolinium cations by 1-benzyl-1,4-dihydronicotinamide. *Can. J. Chem.* **1985**, *63*, 655-662.

(43) Duan, C.; Zhang, J.-F.; Hu, Y.; Zeng, L.; Su, D.; Bao, G.-M. A distinctive near-infrared fluorescence turn-on probe for rapid, sensitive and chromogenic detection of sulfite in food. *Dyes Pigm.* **2019**, 162, 459-465.

(44) Togawa, T.; Ogawa, M.; Nawata, M.; Ogasawara, Y.; Kawanabe, K.; Tanabe, S. High performance liquid chromatographic determination of bound sulfide and sulfite and thiosulfate at their low levels in human serum by pre-column fluorescence derivatization with monobromobimane. *Chem. Pharm. Bull.* **1992,** 40, 3000-3004.

(45) Ji, A. J.; Savon, S. R.; Jacobsen, D. W. Determination of total serum sulfite by HPLC with fluorescence detection. *Clin. Chem.* **1995**, *41*, 897-903.

(46) Kajiyama, H.; Nojima, Y.; Mitsuhashi, H.; Ueki, K.; Tamura, S.; Sekihara, T.; Wakamatsu, R.; Yano, S.; Naruse, T. Elevated Levels of Serum Sulfite in Patients with Chronic Renal Failure. *J. Am. Soc. Nephrol.* **2000**, *11*, 923-927.

(47) Meng, Z.; Li, R.; Zhang, X. Levels of Sulfite in Three Organs from Mice Exposed to Sulfer Dioxide. *Inhalation Toxicol.* **2005**, *17*, 309-313.

(48) Kimura, Y.; Shibuya, N.; Kimura, H. Sulfite protects neurons from oxidative stress. *Br. J. Pharmacol.* **2018**, DOI: 10.1111/bph.14373.

Table of Content